Low-spin $S = \frac{1}{2}$ ground state of the Cu trimers in the paper-chain compound $Ba_3Cu_3In_4O_{12}$

A. A. Gippius, N. E. Gervits, A. V. Tkachev, I. S. Maslova, O. S. Volkova, and A. N. Vasiliev
Low Temperature Physics and Superconductivity Department, Moscow State University, Moscow 119991, Russia

N. Büttgen and W. Kraetschmer
Center for Electronic Correlations and Magnetism EKM, Experimentalphysik V, Universität Augsburg, Augsburg D-86135, Germany

A. S. Moskvin
Department of Theoretical Physics, Institute of Natural Sciences, Ural Federal University, Ekaterinburg 620083, Russia
(Received 25 June 2012; revised manuscript received 21 September 2012; published 9 October 2012)

The magnetic ground states of the isostructural paper-chain compounds $Ba_3Cu_3In_4O_{12}$ and $Ba_3Cu_3Sc_4O_{12}$ were recently found to be ordered antiferromagnetically (AFM), while both quantum magnets reveal positive asymptotic Curie-Weiss temperatures suggestive of ferromagnetic (FM) interactions at high temperatures. Due to the AFM-FM competition the saturation magnetization in both compounds is reached already in modest magnetic fields with a nontrivial succession of two spin-flop and two spin-flip-like transitions in $Ba_3Cu_3In_4O_{12}$. We argue that the paper-chains in both compounds can be described as a system of Cu^I-$2Cu^{II}$ trimers with a low-spin $S = 1/2$ ground state which implies a nonmagnetic spin-singlet Cu^{II} dimer state and a spin-polarized Cu^I ion. To validate the model we performed extensive nuclear resonance—nuclear quadrupole resonance-nuclear magnetic resonance (NQR-NMR)—measurements in $Ba_3Cu_3In_4O_{12}$. Two different types of ^{63,65}Cu nuclear resonance spectra were observed in the magnetically ordered state at zero external magnetic field: (i) a pure NQR spectrum in the frequency range of 24–30 MHz and (ii) a zero-field NMR spectrum in the frequency range of 50–65 MHz. This result unambiguously indicates that one of the two types of copper ions in $Ba_3Cu_3In_4O_{12}$ is in a nonmagnetic spin state below T_N. It provides a unique criterion to test any theoretical model describing the ground-state spin structure in $Ba_3Cu_3In_4O_{12}$. We attribute the pure NQR spectrum to Cu^{II} ions forming nonmagnetic spin-singlet $2Cu^{II}$ dimers and the zero-field NMR spectrum to spin-polarized Cu^I ions. Both NQR and zero-field NMR spectra point to an existence of at least two nonequivalent sets of the copper trimers, probably due to displacements of the Cu^I ions along the cavity in the c direction.

DOI: 10.1103/PhysRevB.86.155114 PACS number(s): 75.10.Jm, 75.10.Pq, 76.60.−k

I. INTRODUCTION

The rich variety of cooperative phenomena in quantum spin systems has triggered a vivid search for new materials with low-dimensional magnetic sublattices. The Cu-O sublattice of $Ba_3Cu_3In_4O_{12}$ consists of a highly unusual arrangement of CuO_4 plaquettes which is unique among the cuprates. Such an arrangement has been described as a so-called paper-chain motif. $Ba_3Cu_3In_4O_{12}$ (Ref. 1) and $Ba_3Cu_3Sc_4O_{12}$ (Ref. 2), together with their solid solutions,[3] were found to be isostructural members of this family.

In terms of coordination polyhedra, buckled Cu^IO_4 plaquettes form vertex-sharing chains in which each plaquette shares four vertices. The chains are constructed such that each buckled Cu^IO_4 plaquette is bridged by two concave $Cu^{II}O_4$ plaquettes linked via opposite oxygen corners of the Cu^IO_4 plaquette. Each successive pair of $Cu^{II}O_4$ plaquettes is rotated by 90° with respect to its predecessor along the c direction. This open-linked chain, shown in Fig. 1 (left panel), represents the paper-chain motif.

At low temperatures, a sharp peak in the temperature dependence of the magnetic susceptibility implies the formation of long-range antiferromagnetic (AFM) order at $T_N = 12.7$ K (Ref. 1) (12.3 K, Ref. 4) and $T_N = 16.0$ K (Ref. 2) (15.2 K, Ref. 4) in $Ba_3Cu_3In_4O_{12}$ and $Ba_3Cu_3Sc_4O_{12}$, respectively. However, at high temperatures, the susceptibility in both compounds follows a Curie-Weiss behavior with a positive, that is, ferromagnetic, Curie-Weiss temperature $\Theta_{CW} = 52$ K (Ref. 1) (56 K, Ref. 4) and 65 K (Ref. 2) (52 K, Ref. 4), respectively. The manifestation of ferromagnetic interactions at high temperature and antiferromagnetic ordering at low temperature in these compounds motivated further investigations. The transition to the magnetically ordered state of $Ba_3Cu_3In_4O_{12}$ (Ref. 1) and $Ba_3Cu_3Sc_4O_{12}$ (Ref. 2) yields quite pronounced typical anomalies at T_N and some unexpected features in the specific heat. The magnetic heat capacity, obtained from C_p by subtracting the lattice contribution in $Ba_3Cu_3Sc_4O_{12}$ (Ref. 2), has a broad maximum at about 30 K which suggests the existence of a magnetic contribution to the heat capacity at temperatures much higher than T_N. The observed entropy change due to the AFM ordering is found to be much smaller than that expected for $S = 1/2$ systems (Rln2) in both $Ba_3Cu_3In_4O_{12}$ and $Ba_3Cu_3Sc_4O_{12}$ (Refs. 1 and 2). In addition to the anomalies at T_N in both $Ba_3Cu_3In_4O_{12}$ and $Ba_3Cu_3Sc_4O_{12}$ (Refs. 1,2), there are also broad Schottky-type maxima in the C_p/T vs T data around 5 K [$Ba_3Cu_3In_4O_{12}$ (Ref. 1)] and 3 K [$Ba_3Cu_3Sc_4O_{12}$ (Ref. 2)] pointing to an extra contribution to the entropy.

The μSR data for $Ba_3Cu_3Sc_4O_{12}$ (Ref. 2) taken in zero applied magnetic field provide strong evidence for a conventional magnetic ordering and point to an occurrence of magnetically nonequivalent sites, attributed by the authors to a probable existence of multiple muon trapping sites.

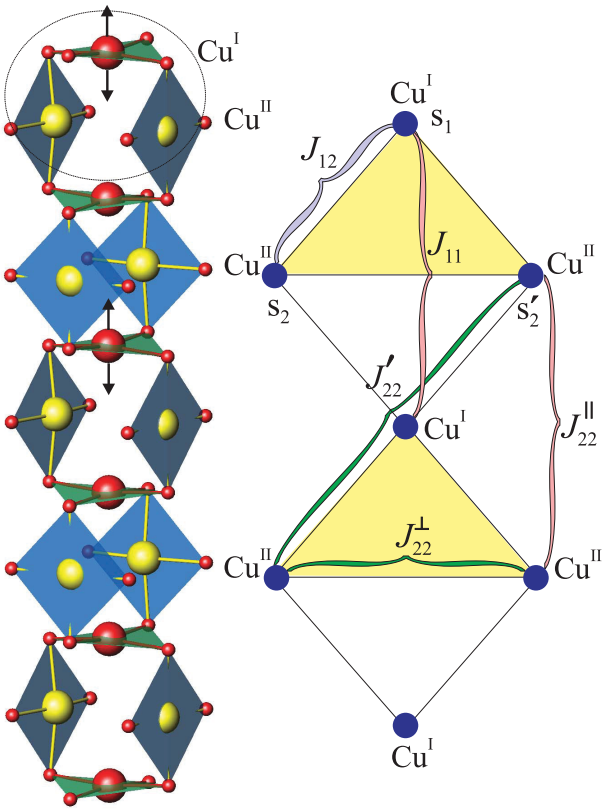

FIG. 1. (Color online) Fragment of the paper-chain column (left) and the Cu^{I}-$2Cu^{II}$ trimers (right) in $Ba_3Cu_3In_4O_{12}$. The paper-chain column consists of vertex-sharing buckled $Cu^{I}O_4$ (horizontal) and concave $Cu^{II}O_4$ (vertical) units. Large spheres represent the Cu^{2+}; small spheres are the O^{2-} ions. Arrows mark soft-mode displacements of the Cu^{I} ions across the cavity in the c direction. The encircled three Cu ions compose one of the Cu^{I}-$2Cu^{II}$ trimers. The right panel represents a planar scheme of the paper-chain column with the Cu^{I}-$2Cu^{II}$ trimers set off with shading. Shown are the spins of the Cu ions in the trimer and main exchange paths. The J_{12} is a main intratrimer Cu^{I}-Cu^{II} exchange integral, $J_{22}^{\perp}$ is a intratrimer Cu^{II}-Cu^{II} exchange integral, J_{11} is a intertrimer Cu^{I}-Cu^{I} exchange integral, and $J_{22}^{\parallel}$ and J'_{22} are intertrimer Cu^{II}-Cu^{II} exchange integrals.

The above results clearly suggest that $Ba_3Cu_3In_4O_{12}$ and $Ba_3Cu_3Sc_4O_{12}$ must have significant three-dimensional magnetic interactions which lead to the observed long-range magnetic order. Furthermore, these observations indicate the presence of competing magnetic interactions leading to frustration.

As one of the most striking signatures of the AFM and FM competition in the paper-chain antiferromagnets $Ba_3Cu_3In_4O_{12}$ and $Ba_3Cu_3Sc_4O_{12}$ we point to a very low magnitude of the magnetic field $\mu_0 H_S$ necessary to saturate the magnetization, that is, 5 T in $Ba_3Cu_3In_4O_{12}$ and 8 T in $Ba_3Cu_3Sc_4O_{12}$, respectively.[1,2,4] Furthermore, sharp additional singularities in the derivatives dM/dB related to spin-flop-like and spin-flip-like transitions were clearly seen at several critical fields $H < H_S$ for $T < T_N$ by other authors.

The dramatic sensitivity of the Néel temperature to an applied magnetic field (a field of 7 T was sufficient to decrease the T_N from 16 K to zero[2]) is somewhat puzzling and also indicates the presence of competing interactions.

A neutron diffraction study of $Ba_3Cu_3Sc_4O_{12}$ (Ref. 2) has revealed a complex magnetic order at low temperatures with a commensurate propagation vector $\mathbf{k} = (010)$, which is greatly influenced by an external magnetic field. The ordering is found to be antiferromagnetic with the magnetic moments at the Cu^{I} and Cu^{II} sites probably aligned opposite to each other. The neutron scattering experiment on $Ba_3Cu_3In_4O_{12}$ is hampered by the high absorption cross section of indium. A simple qualitative picture of the magnetic order in this compound with three virtually independent orthogonal antiferromagnetic spin orderings at the Cu^{I} and Cu^{II} sites has been recently suggested in Ref. 1.

However, both these model suggestions, as well as all the unconventional properties of the new paper-chain compounds, require further theoretical and experimental examination.

Local probes such as nuclear quadrupole resonance (NQR) and nuclear magnetic resonance (NMR) enable us to obtain a deeper insight into the system giving fine details which are not accessible in bulk thermodynamic probe data. The NQR and NMR techniques proved to be an effective tool for the study of different cuprates with various types of the CuO_4 plaquette arrangement and complex spin structures (see, e.g., Refs. 5). Fortunately, $Ba_3Cu_3In_4O_{12}$ contains many NQR-active nuclei (listed in Table I below) providing a unique opportunity to probe the local crystal and electronic surroundings at several crystallographic sites.

In Sec. II we present a theoretical analysis of different exchange paths within the paper chains and argue that these form a chain system of Cu^{I}-$2Cu^{II}$ trimers with a bare low-spin $S = 1/2$ ground state which implies a nonmagnetic spin-singlet Cu^{II} dimer state. To validate this model we performed extensive nuclear resonance NQR-NMR measurements for the copper, indium, and barium nuclei in $Ba_3Cu_3In_4O_{12}$. Experimental results with discussions are presented in Sec. III. A summary and conclusions are made in Sec. IV.

II. Cu^{I}-$2Cu^{II}$-trimers in $Ba_3Cu_3In_4O_{12}$

The spin structure of $Ba_3Cu_3In_4O_{12}$ is determined by the Cu^{I} ions and $2Cu^{II}$ dimers forming the paper-chain motif; however, the paper chains can be represented to be a regular system of exchange-coupled Cu^{I}-$2Cu^{II}$ trimers (see Fig. 1) with the trimer planes of nearest neighbors oriented orthogonal to each other. This basic element of the paper-chain structure incorporates the two main competing exchange interactions, that is, the ferromagnetic Cu^{I}-Cu^{II} exchange (J_{12}) and the antiferromagnetic Cu^{II}-Cu^{II} exchange ($J_{22}^{\perp}$) (see Ref. 2). The Heisenberg exchange Hamiltonian for an isolated Cu^{I}-$2Cu^{II}$ trimer can be written as follows:

$$\hat{H}_{ex} = J_{22}^{\perp}(\hat{\mathbf{s}}_2 \cdot \hat{\mathbf{s}}'_2) + J_{12}(\hat{\mathbf{s}}_1 \cdot \hat{\mathbf{S}}_2), \tag{1}$$

where

$$\hat{\mathbf{S}}_2 = \hat{\mathbf{s}}_2 + \hat{\mathbf{s}}'_2.$$

In terms of a net trimer spin $\hat{\mathbf{S}} = \hat{\mathbf{S}}_2 + \hat{\mathbf{s}}_1$ we can rewrite $\hat{H}_{ex}$ as follows:

$$\hat{H}_{ex} = \tfrac{1}{2} J_{22}^{\perp}\left[\hat{\mathbf{S}}_2^2 - \tfrac{3}{2}\right] + \tfrac{1}{2} J_{12}\left[\hat{\mathbf{S}}^2 - \hat{\mathbf{S}}_2^2 - \tfrac{3}{4}\right]. \tag{2}$$

Eigenvalues, or the trimer energy spectrum, can be easily obtained if we take into account that $\hat{\mathbf{S}}_i^2 \to S_i(S_i + 1)$ and

TABLE I. NQR-active nuclei in $Ba_3Cu_3In_4O_{12}$.

Nucleus	Spin	$\gamma/2\pi$ (MHz/T)	$2\pi/\gamma$ (T/MHz)	NA (%)	Q (10^{-24} cm^2)	NQR transitions	$Ba_3Cu_3In_4O_{12}$(this work)
^{63}Cu	3/2	11.28	0.0887	69.2	−0.222	$\pm1/2 \leftrightarrow \pm3/2$	+
^{65}Cu	3/2	12.09	0.0827	30.8	−0.195	$\pm1/2 \leftrightarrow \pm3/2$	+
						$\pm1/2 \leftrightarrow \pm3/2$	+
^{115}In	9/2	9.33	0.107	95.7	0.83	$\pm3/2 \leftrightarrow \pm5/2$	+
						$\pm5/2 \leftrightarrow \pm7/2$	+
						$\pm7/2 \leftrightarrow \pm9/2$	+
^{135}Ba	3/2	4.23	0.236	6.59	0.18	$\pm1/2 \leftrightarrow \pm3/2$	−
^{137}Ba	3/2	4.73	0.211	11.32	0.28	$\pm1/2 \leftrightarrow \pm3/2$	+

$s_2 = s_2' = s_1 = \frac{1}{2}$:

$$E(S_2S) = \tfrac{1}{2}J_{12}S(S+1) + \tfrac{1}{2}(J_{22}^{\perp} - J_{12})S_2(S_2+1) - \tfrac{3}{8}(2J_{22}^{\perp} + J_{12}). \quad (3)$$

Eigenvectors $|S_2SM\rangle$ (ket vectors) have a standard form:

$$|S_2SM\rangle = \sum_{M_2m} \begin{bmatrix} S_2 & \frac{1}{2} & S \\ M_2 & m & M \end{bmatrix} |S_2M_2\rangle \left|\frac{1}{2}m\right\rangle, \quad (4)$$

where $[\,\cdot\,\cdot\,\cdot\,]$ is a Clebsch-Gordan coefficient, $|S_2M_2\rangle$ and $|\frac{1}{2}m\rangle$ are the eigenvectors of $\hat{\mathbf{S}}_2^2$, $\hat{S}_{2z}$ and $\hat{\mathbf{s}}_1^2$, $\hat{s}_{1z}$, respectively. Possible values of the intermediate spin S_2, or the $2Cu^{II}$-dimer spin, are $S_2 = 0$ and $S_2 = 1$, while for the net trimer spin we obtain $S = \frac{1}{2}$ at $S_2 = 0$ or $S = \frac{1}{2}$ and $S = \frac{3}{2}$ at $S_2 = 1$. The three-level $[E(0\frac{1}{2})$, $E(1\frac{1}{2})$, and $E(1\frac{3}{2})]$ trimer energy spectrum is shown in Fig. 2 given a negative (ferromagnetic) sign of J_{12} in units of $|J_{12}|$ as a function of $J_{22}^{\perp}$ taken also in units of $|J_{12}|$. It should be noted that for $J_{22}^{\perp} < \frac{1}{2}|J_{12}|$ the Cu^I-$2Cu^{II}$ trimer has a ferromagnetic high-spin (HS) ground state ($S = \frac{3}{2}$), while for $J_{22}^{\perp} > \frac{1}{2}|J_{12}|$ the HS FM ground state is replaced with a low-spin (LS) $S = \frac{1}{2}$ ground state produced by the nonmagnetic $S_2 = 0$ singlet $2Cu^{II}$ dimer state. In other words, spin magnetism in this state is governed only by the $s_1 = \frac{1}{2}$ spin. Hence, the in-chain low-temperature magnetic behavior in the trimer system will be determined only by the Cu^I-Cu^I exchange integral J_{11} (see Fig. 1). The formation of the spin singlets at the Cu^{II} ions does exclude magnetic frustration in paper-chain systems as it was already discarded in the orthogonal spin ordering model proposed in Ref. 1.

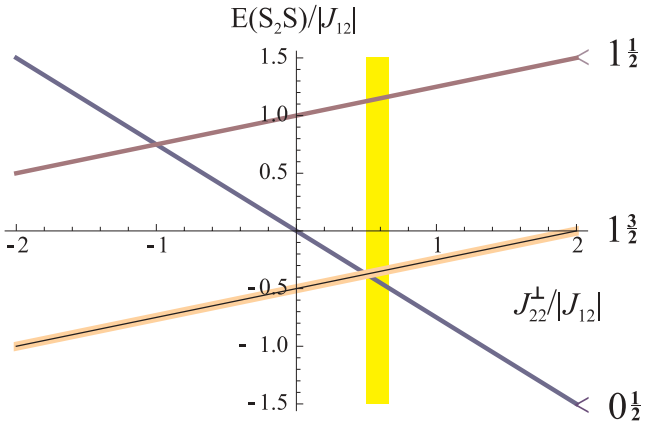

FIG. 2. (Color online) Energy spectrum of an isolated Cu^I-$2Cu^{II}$ trimer in $Ba_3Cu_3In_4O_{12}$ ($J_{12} < 0$, energy in units of $|J_{12}|$). The shaded area marks the range of the $J_{22}^{\perp}/|J_{12}|$ ratios as estimated in Ref. 2. Small splitting due to a spin anisotropy is shown by a thickening of the $S = \frac{3}{2}$ level. Numbers on the right mark the values of S_2 and S, respectively.

It is worth noting that the two-ion anisotropy, or anisotropic exchange, works only for the HS $S = \frac{3}{2}$ state, giving rise to its splitting into two Kramers doublets. In Fig. 2 this effect is shown by a thickening of the $S = \frac{3}{2}$ level. Interestingly, the magnetic moment of the Cu^I ion in the isolated trimer appears to be of $\pm1\mu_B$, $\pm1\mu_B$, $\pm\frac{1}{3}\mu_B$, and $\mp\frac{1}{3}\mu_B$ for the $|0\frac{1}{2} \pm \frac{1}{2}\rangle$, $|1\frac{3}{2} \pm \frac{3}{2}\rangle$, $|1\frac{3}{2} \pm \frac{1}{2}\rangle$, and $|1\frac{1}{2} \pm \frac{1}{2}\rangle$ doublets, respectively. It should be noted that the anisotropy axes (planes) for the adjacent trimers are interlinked by the C_4 transformation.

Theoretical estimates of different Cu-Cu exchange integrals are available for the isostructural cuprate $Ba_3Cu_3Sc_4O_{12}$ (Ref. 2): $J_{12} \approx (-12.4)$–(-14.6); $J_{22}^{\perp} \approx 6.9$–$8.2$; $J_{22}^{\parallel} \approx 2.5$–$10.5$; $J_{11} \approx 2.7$–5.6 meV. These values convincingly point to a ferromagnetic sign of J_{12} and antiferromagnetic sign of $J_{22}^{\perp}$, with the ratio $J_{22}^{\perp}/|J_{12}|$ slightly above 1/2 for a rather wide range of the correlation parameter $4 < U_d < 8$ eV (see Fig. 2). In other words, theoretical estimates[2] point to a LS $S = \frac{1}{2}$ ground state of the Cu^I-$2Cu^{II}$ trimer produced by the nonmagnetic $S_2 = 0$ singlet $2Cu^{II}$-dimer state, however, only slightly separated from the HS ferromagnetic $S = \frac{3}{2}$ state. As an important indication to the $\frac{1}{2}$–$\frac{3}{2}$ quasidegeneracy one should point to results of the electron spin resonance (ESR) measurements in $Ba_3Cu_3In_4O_{12}$ (Ref. 1), which revealed a spin gap of 63 GHz ≈ 3 K.

The LS-HS ($\frac{1}{2}$–$\frac{3}{2}$) quasidegeneracy would immediately give rise to a low-temperature Schottky-type anomaly in the specific heat. Making use of a familiar expression,

$$c = \frac{R}{T^2}(\langle E^2\rangle - \langle E\rangle^2), \quad (5)$$

we can easily calculate the specific heat for an isolated Cu^I-$2Cu^{II}$ trimer. For illustration we show the temperature dependence of the specific heat of a Cu^I-$2Cu^{II}$ trimer with isotropic exchange at $J_{22}^{\perp}/|J_{12}| = 0.6$ in Fig. 3. Two distinctive features are readily visible: a sharp low-temperature Schottky-type anomaly and a high-temperature broad maximum. It is worth noting that the anisotropic splitting of a $S = 3/2$ quartet would result in smearing out the Schottky anomaly. The low-temperature Schottky-type anomaly was indeed observed both in $Ba_3Cu_3Sc_4O_{12}$ at $T_S \approx 3$ K (Ref. 2) and $Ba_3Cu_3In_4O_{12}$

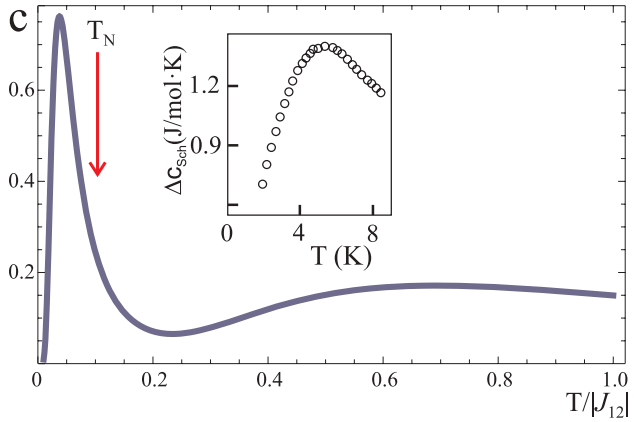

FIG. 3. (Color online) Temperature dependence of the specific heat for an isolated Cu^{I}-$2Cu^{II}$ trimer with fixed ratio $J_{22}^{\perp}/|J_{12}| = 0.6$ (T in units of $|J_{12}|$). The inset shows the Schottky-type anomaly in $Ba_3Cu_3In_4O_{12}$ as received from experiment.[1]

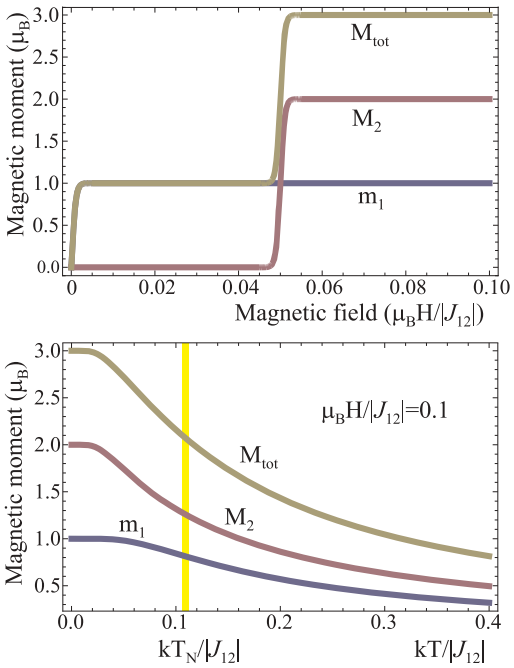

FIG. 4. (Color online) (Top) Magnetization curve for an isolated Cu^{I}-$2Cu^{II}$ trimer in paper-chain compounds with the partial contributions of the Cu^{I} and Cu^{II} ions ($T/|J_{12}| = 0.01$, Zeeman energy $\mu_B H$ in units of $|J_{12}|$). (Bottom) Temperature dependence of the magnetization for an isolated Cu^{I}-$2Cu^{II}$ trimer in paper-chain compounds with the partial contributions of Cu^{I} and Cu^{II} ions (Zeeman energy $\mu_B H = 0.1$ in units of $|J_{12}|$). The shaded area marks T_N in relative units.

at $T_S \approx 5$ K (Ref. 1). A broad maximum at about 30 K has been clearly observed in $Ba_3Cu_3Sc_4O_{12}$ (Ref. 2).

Interestingly, the experimentally known position of the Schottky anomaly enables us to estimate the Cu^{I}-Cu^{II} exchange integral. Given $J_{22}^{\perp}/|J_{12}| = 0.6$ and $T_S \approx 5\ \mathrm{K} \approx 0.04|J_{12}|$ (see Fig. 3), we arrive at $|J_{12}| \approx 125\ \mathrm{K} = 11.4$ meV, which nicely agrees with theoretical estimates for $Ba_3Cu_3Sc_4O_{12}$ (Ref. 2). In turn, this value enables us to find the relative magnitude of $T_N = 12.7\ \mathrm{K} : k_B T_N/|J_{12}| \approx 0.1$ (see Fig. 3).

So, the relatively low value of T_N has a simple explanation: The very strong Cu^{I}-Cu^{II} and Cu^{II}-Cu^{II} exchange interactions generating the LS ground state of the Cu trimer do not contribute to T_N, which is determined by weaker intrachain and interchain exchange couplings.

In Fig. 4 we present the magnetization $M(H)$ and $M(T)$ dependencies (top and bottom panels, respectively) for an isolated Cu^{I}-$2Cu^{II}$ trimer with isotropic spin exchange in $Ba_3Cu_3In_4O_{12}$ with the partial contributions of the Cu^{I} and Cu^{II} ions, m_1 and M_2, respectively. Note the characteristic two-step magnetization curve. For $\mu_B H/|J_{12}| \leqslant 0.05$ the magnetization is determined only by the Cu^{I} contribution while at $\mu_B H/|J_{12}| \geqslant 0.05$ the trimer ground state changes from the LS to the HS one. Given the above estimates for J_{12} we arrive at a rather large value of the critical spin-flip field of $\mu_0 H_{sf} \approx 9$ T, typical for $Ba_3Cu_3Sc_4O_{12}$ rather than for $Ba_3Cu_3In_4O_{12}$. It means that the ratio $J_{22}^{\perp}/|J_{12}|$ for the latter should be closer to the critical value of 0.5.

Anisotropic exchange can give rise to a three-step magnetization due to a splitting of the HS $S = 3/2$ state. Hence, the intrinsic spin structure of the isolated Cu^{I}-$2Cu^{II}$ trimer points to an occurrence of at least three particular magnetic fields related with a step-by-step change of the trimer ground state. Obviously in a bulk system of the Cu^{I}-$2Cu^{II}$ trimers these singularities turn into a series of spin-flop- and spin-flip-like phase transitions indeed observed in $Ba_3Cu_3In_4O_{12}$ below T_N (Ref. 1).

In the bottom panel of Fig. 4 we show the AFM ordering temperature $kT_N \approx 0.1|J_{12}|$ and we see that the specific trimer structure will give rise to remarkable short-range order effects well above the ordering temperature.

All these implications of our Cu^{I}-$2Cu^{II}$-trimer model provide strong evidence that the LS-HS quasidegeneracy is a fingerprint of paper-chain compounds and accounts for their experimentally observed unconventional magnetic and electronic properties.

III. EXPERIMENTAL AND DISCUSSION

The barium-copper indate $Ba_3Cu_3In_4O_{12}$ crystallizes in the tetragonal $I4/mcm$ space group with lattice parameters $a = 12.121(3)$ Å, $c = 8.511(4)$ Å, $V = 1250(2)$ Å^3, $c/a = 0.70$.[6,7] Our $Ba_3Cu_3In_4O_{12}$ polycrystalline sample was synthesized by a high-temperature solid-state reaction of stoichiometric amounts of $BaCO_3$, CuO, and In_2O_3. The component binary phases were ground, pelleted, and fired in alumina crucibles at 850 °C–950 °C in air for 72 h with regrinding every 24 h. The samples were quench cooled in air to room temperature. The phase purity of the sample obtained was confirmed by powder x-ray diffraction using a RADIAN-2 diffractometer with CuK_α radiation over a 2θ range of 20°–60°.

NQR and zero-field NMR spectra were measured by means of the home-built phase coherent pulsed spectrometer using a frequency step point-by-point spin-echo technique at temperatures $1.6 < T < 15$ K and $T = 1.6$ K, respectively. Typical pulse lengths were 2–5 and 4–10 μs for the $\pi/2$ and π pulses, respectively, with a pulse separation of 15–100 μs, depending on nucleus, temperature, and type of experiment.

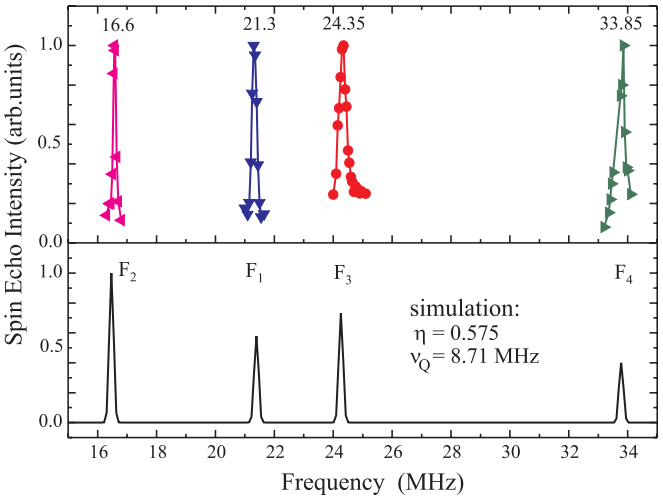

FIG. 5. (Color online) (Top) Experimental ^{115}In NQR spectrum of $Ba_3Cu_3In_4O_{12}$ measured at 4.2 K. The intensity of each NQR line is normalized to its maximum value. (Bottom) Simulated ^{115}In spectrum with parameters $\eta = 0.575$ and $\nu_Q = 8.71$ MHz. Frequencies F_1–F_4 stand for the NQR transitions $\pm 1/2 \leftrightarrow \pm 3/2$, $\pm 3/2 \leftrightarrow \pm 5/2$, $\pm 5/2 \leftrightarrow \pm 7/2$, and $\pm 7/2 \leftrightarrow \pm 9/2$, respectively.

NMR spectra were recorded by sweeping the magnetic field at several fixed frequencies. In any nuclear resonance experiment the area under the spin-echo magnitude was integrated in the time domain and averaged over the scan accumulation number, which depends on the nucleus.

A. NQR

1. ^{115}In NQR spectrum

We start presenting our experimental NQR results with the ^{115}In NQR spectrum measured at 4.2 K (Fig. 5, top). It consists of four sharp NQR lines F_1–F_4 with a full width at half maximum (FWHM) of about 200 kHz corresponding to four NQR transitions of the $I = 9/2$ nuclei: $\pm 1/2 \leftrightarrow \pm 3/2$, $\pm 3/2 \leftrightarrow \pm 5/2$, $\pm 5/2 \leftrightarrow \pm 7/2$, and $\pm 7/2 \leftrightarrow \pm 9/2$, respectively. Since the lines are distributed over a wide frequency range of 16–34 MHz, different RF coils were required for measuring each line. Therefore, the intensity of each line in Fig. 5 (top) was normalized to its maximum value.

The Hamiltonian of the nuclear quadrupole interaction is given by

$$\hat{H}_Q = \frac{eQV_{zz}}{4I(2I-1)}\left[\left(3\hat{I}_z^2 - \hat{\mathbf{I}}^2\right) + \eta\left(\hat{I}_x^2 - \hat{I}_y^2\right)\right], \qquad (6)$$

where V_{zz} is the largest eigenvalue of the electric field gradient (EFG) tensor, I is the nuclear spin, and η the asymmetry parameter. As follows from Eq. (6), the frequencies of the NQR transitions are proportional to the quadrupole frequency $\nu_Q = eQV_{zz}/2hI(2I-1)$, which is *a priori* unknown and strongly depends on the asymmetry parameter which characterizes the deviation of the local site symmetry from an axial one. To perform an accurate NQR line assignment and to avoid any dependence on ν_Q we compared the ratios of the observed NQR transition F_i/F_1 ($i = 2$–4) frequencies with the one obtained by numerical solution of the quadrupole Hamiltonian (6) as a function of η. Finally, we got an η value of $\eta = 0.57$, which we used as a starting parameter for the spectrum simulation by means of the SIMUL program which performs a direct numerical solution of the spin-Hamiltonian including, in general, both the Zeeman and quadrupole parts. The resulting simulated ^{115}In NQR spectrum ($\eta = 0.575$, $\nu_Q = 8.71$ MHz) is presented in Fig. 5 (bottom) showing very good agreement with the experimental NQR lines.

It is worth noting that the EFG for ^{115}In in $Ba_3Cu_3In_4O_{12}$ is about ten times stronger than for ^{45}Sc, occupying the same position in isostructural $Ba_3Cu_3Sc_4O_{12}$ (Ref. 2) ($\nu_Q \leqslant$ 0.4 MHz). Such a difference reflects a stronger distortion of the InO_6 octahedra in $Ba_3Cu_3In_4O_{12}$ than the ScO_6 octahedra in $Ba_3Cu_3Sc_4O_{12}$ (Ref. 3).

Astonishingly, we did not find any magnetic splitting of the NQR lines which proves that there are only negligible contributions of either supertransferred or dipolar magnetic fields at the indium site in the magnetically ordered state at 4.2 K in $Ba_3Cu_3In_4O_{12}$. It is rather unexpected since from the crystal structure it appears that ^{115}In is hyperfine coupled to three Cu ions which are part of a spin-polarized Cu^I-$2Cu^{II}$ trimer.

In addition, we followed the temperature evolution of the two ^{115}In NQR lines F_1 ($\pm 1/2 \leftrightarrow \pm 3/2$ transition) and F_2 ($\pm 3/2 \leftrightarrow \pm 5/2$ transition). The temperature dependencies of these NQR lines are presented in Fig. 6. Both temperature dependencies of F_1 and F_2 exhibit a sharp kink in the vicinity of T_N. Moreover, F_1 and F_2 shift rapidly below T_N, however, in strictly opposite directions. Such an unusual shift of the ^{115}In NQR lines accompanied by the change of their intensity and line shape, particularly pronounced for the $F_2(T)$ line at 8.0 K [see Fig. 6(d)], points to fluctuations of a dynamic EFG tensor which coexist with the long-range magnetic order.

This phenomenon may be related to (quasi)static nonuniform displacements of the Cu^I ions across the cavity in the c direction. Such a distortion accompanied with a buckling of the Cu^IO_4 plaquettes seems to be a soft mode for $Ba_3Cu_3In_4O_{12}$. Indeed, the thermal parameters U for Cu^I ions in $Ba_3Cu_3In_4O_{12}$ surpass those for the Cu^{II} and oxygen ions by more than 30 times.[3] The giant "blue shift" of the line F_1 amounts to $\Delta\nu_1/\nu_1 \approx 7\%$ [see Fig. 6(a)] and evidences a huge magnitude of local "magnetostrictive" distortions in the

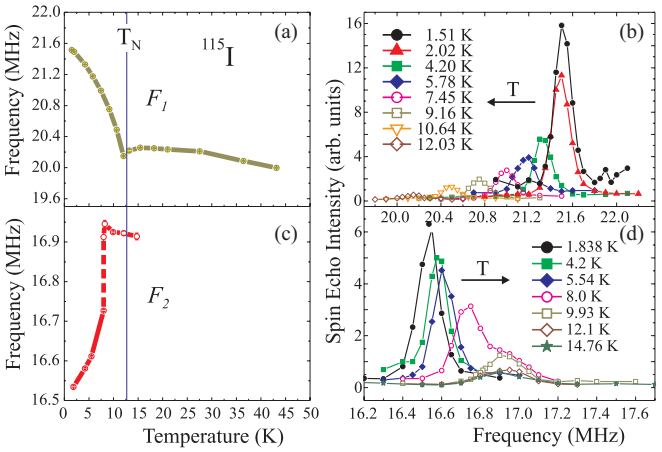

FIG. 6. (Color online) Temperature evolution of the ^{115}In NQR lines F_1 (a),(b) and F_2 (c), (d). Solid lines are guides to the eye.

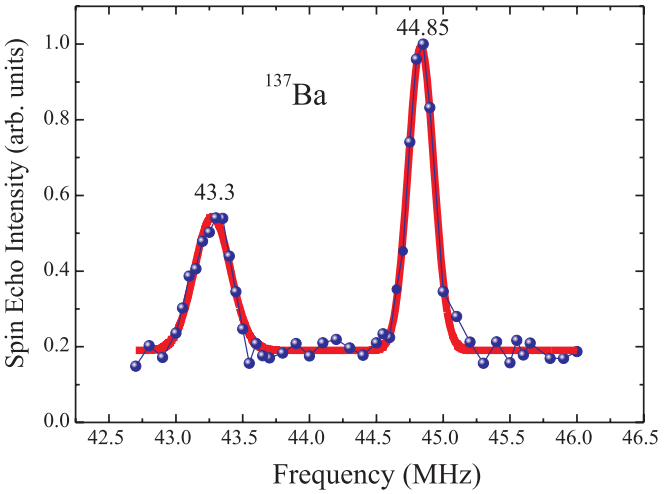

FIG. 7. (Color online) ^{137}Ba NQR spectrum of $Ba_3Cu_3In_4O_{12}$ measured at 4.2 K (see text). Solid lines is the best fit by Gaussian lines.

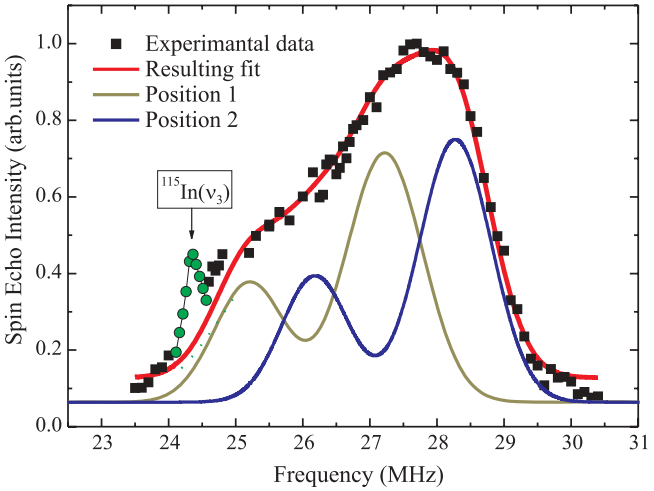

FIG. 8. (Color online) ^{63,65}Cu NQR spectrum of $Ba_3Cu_3In_4O_{12}$ measured at 4.2 K. The solid lines correspond to Gaussian best fits of the ^{65}Cu and ^{63}Cu isotopes for the both Cu^{II} positions, assuming a quadrupole character of the line broadening (see text). The thickest solid line is the resulting best fit.

$Ba_3Cu_3In_4O_{12}$ structure (probably both in Cu^I-O-In bonds and angles) below T_N.

2. ^{135,137}*Ba NQR spectrum*

Since there are two nonequivalent crystallographic positions of Ba in the $Ba_3Cu_3In_4O_{12}$ crystal structure[3] and two barium isotopes ^{135}Ba and ^{137}Ba (see Table I) one expects to observe four different Ba NQR lines. However, we found only two relatively weak solitary NQR lines near 44 MHz with almost equal integral intensities and a factor of two difference in the linewidth (Fig. 7). The first task is to assign these lines. The ratio of their resonance frequencies is about 1.04, which is much less than the ratio of quadrupole moments of the two Ba isotopes $^{137}Q/^{135}Q = 1.56$ (see Table I). Therefore, the observed two NQR lines most likely originate from two nonequivalent crystallographic Ba positions occupied by one Ba isotope, which has to be identified. If it was ^{135}Ba the second pair of lines from ^{137}Ba should be observed in the higher frequency range of about 67–70 MHz. We did not find a NQR signal there. So we conclude that the observed pair of NQR lines belongs to the ^{137}Ba isotope. Both barium atoms in $Ba_3Cu_3In_4O_{12}$ are coordinated to oxygen in a cuboctahedral geometry with the bonding environment around Ba(2) more distorted than that of Ba(1) (Ref. 3). The high-energy and low-energy ^{137}Ba NQR lines may be attributed to these Ba sites, respectively. Interestingly, the two ^{137}Ba NQR lines resemble both in the frequency and linewidth the ^{137}Ba NQR line in the insulating cuprate $YBa_2Cu_3O_{6.05}$ (Ref. 8). As in this 123 cuprate we cannot exclude an internal magnetic field present at the Ba sites in $Ba_3Cu_3In_4O_{12}$ with a magnitude on the order of 0.01 T.

The ^{135}Ba lines should be situated in the frequency range of 27.5–30 MHz. Unfortunately, due to the even poorer natural abundance of the ^{135}Ba isotope these lines seem to be completely hidden beneath a strong and broad NQR line (Fig. 8), occupying the frequency range of 24–30 MHz, which can be explicitly attributed to the ^{63,65}Cu NQR spectrum.

3. ^{63,65}*Cu NQR spectrum*

The frequency range of 24–30 MHz turned out to be typical for the ^{63,65}Cu nuclei in the CuO_4 plaquettes in different cuprates. However, the ^{63,65}Cu NQR FWHM (see Fig. 8) is much larger than typical copper NQR linewidths in other cuprates including $La_{2-x}Sr_xCuO_4$ with a record FWHM of 0.6–2 MHz for nonzero x (Ref. 9). The narrow line F_3 of the ^{115}In nuclei observed at the left-hand side of the copper spectrum provides a striking illustration of the unusual ^{63,65}Cu NQR linewidth in $Ba_3Cu_3In_4O_{12}$. The origin of this line broadening could be either magnetic caused by local magnetic fields induced at the Cu site or electric due to an inhomogeneous distribution of EFGs in space.

We fitted the experimental copper NQR spectrum with two pairs of Gaussian lines with equal integral intensities (blue and olive solid lines in Fig. 8). For each pair of lines the ratio of the central frequencies and the intensities is equal to the ratio of the quadrupole moments and the natural abundances of the ^{63}Cu and ^{65}Cu isotopes, respectively (see Table I). For the case of a magnetic mechanism of the line broadening the ^{65}Cu line should be approximately 10% broader due to the slightly higher gyromagnetic ratio of ^{65}Cu:$^{65}\gamma/^{63}\gamma = 1.072$. The resulting fit obtained for this situation was not satisfactory. In contrast, for the case of a quadrupole origin of the line splitting, the ^{65}Cu FWHM should be approximately 10% narrower reflecting the lower quadrupole moment of ^{65}Cu: $^{65}Q/^{63}Q = 0.878$. The best fit for the latter case with quadrupole frequencies and linewidths for ^{63}Cu NQR lines of 27.2 (28.3) MHz and 1.13 (1.07) MHz in positions 1 (2) is depicted in Fig. 8.

Again, as for ^{115}In NQR, we did not find a magnetic splitting of the ^{63,65}Cu NQR lines. It means that here we observe nonmagnetic copper ions, or, strictly speaking, Cu ions for which $\langle \mathbf{S} \rangle = 0$. Such a result is consistent with our model of a LS ground state of the Cu^I-$2Cu^{II}$ trimer. In other words, the ^{63,65}Cu NQR spectrum in the range of 24–30 MHz

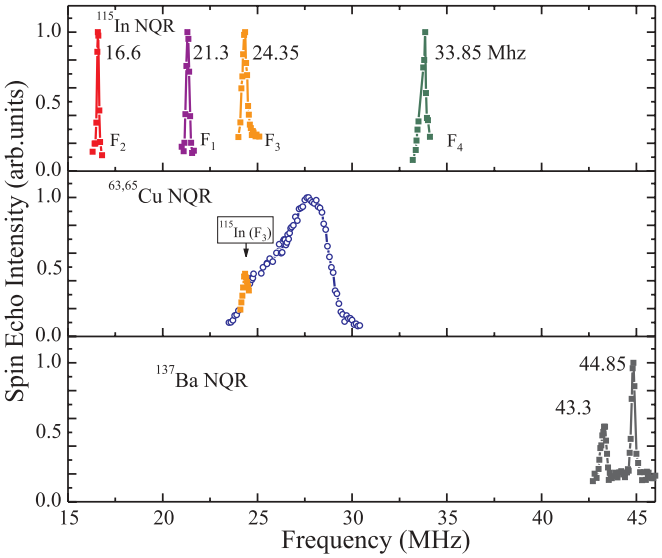

FIG. 9. (Color online) Summary of the observed NQR spectra measured at 4.2 K.

can be attributed to Cu^{II} ions which form the nonmagnetic spin-singlet $2Cu^{II}$ dimer.

The doublet structure of the ^{63,65}Cu NQR spectrum is assumed to be a direct effect of quasistatic displacements of Cu^{I} ions along the cavity in the c direction[3] accompanied by the emergence of two nonequivalent $2Cu^{II}$ dimers located above and below the mobile Cu^{I} ion (see Fig. 1).

Summarizing our NQR results obtained at 4.2 K in the frequency range of 15–45 MHz we plotted all observed NQR spectra in Fig. 9.

4. Spin-spin relaxation measurements

An additional, independent verification of the absence of a magnetic field at the In and Cu^{II} sites is provided by spin-spin relaxation measurements at $T = 2.5$ K in which the spin-echo intensity $M(\tau)$ was measured as a function of the spacing τ between the $\pi/2$ and π pulses in the spin-echo pulse sequence. We performed these experiments for the F_1 and F_2 NQR lines of ^{115}In as well as for $^{63,65}Cu^{II}$ NQR in the magnetically ordered state of $Ba_3Cu_3In_4O_{12}$. The results are shown in Fig. 10 (top). The decay of the spin-echo intensity can be expressed as

$$M(\tau) = M(0)\exp\left(-\frac{2\tau}{T_{2R}}\right)\exp\left(-\frac{(2\tau)^2}{2T_{2G}^2}\right), \qquad (7)$$

where the first exponential term represents the Redfield contribution T_{2R} caused by the spin-lattice interaction and the second term is the Gaussian decay function due to the spin-spin interaction. As seen from Fig. 10, the spin-echo decay functions for the $^{63}Cu^{II}$ and ^{115}In nuclei look different. For $^{63}Cu^{II}$ the $M(\tau)$ decay contains only the Redfield contribution and is very fast with $T_{2R} \sim 50$ μs even at such a low temperature (2.5 K), indicating a strong coupling to the rapidly fluctuating electronic system. In contrast, for both ^{115}In NQR lines we observed exclusively a Gaussian type of spin-echo decay which is relatively slow with $T_{2G} \sim 760$ μs and 1000 μs for the F_1 and F_2 ^{115}In NQR lines, respectively. The most important result of these spin-spin relaxation experiments is the absence of any visible oscillations in the $M(\tau)$ curves of the $^{63}Cu^{II}$ and ^{115}In NQR lines.

This provides unambiguous evidence for a negligible value of any local magnetic fields at the Cu^{II} and In sites in $Ba_3Cu_3In_4O_{12}$ in the case of zero applied magnetic field. Indeed, the presence of a small magnetic field $H_{\rm loc}$ at the nuclear site leads to a modulation of the magnetization decay function,[11,12] which in general is given by

$$M(\tau) = M(0)\exp\left(-\frac{2\tau}{T_2}\right) \times \left[1 - K\exp\left(-\frac{2\tau}{T_2''}\right)\cos(2\tau\omega_{\rm mod} + \phi)\right], \qquad (8)$$

where $\omega_{\rm mod} = \gamma_n H_{\rm loc}$ is the modulation frequency, $M(0)$, K, T_2'', and ϕ are the fitting parameters.[8] Such a modulation was observed, for example, in the antiferromagnetic $YBa_2Cu_3O_{6.05}$ for the ^{137}Ba spin-echo decay detecting a local field $H_{\rm loc}$ value of $\mu_0 H_{\rm loc} = 1.54 \times 10^{-2}$ T at the Ba site at 16 K (Ref. 8). The magnetization decay for the ^{137}Ba NQR line at 44.9 MHz is shown in Fig. 10, bottom panel. In contrast to that for the $^{63}Cu^{II}$ and ^{115}In NQR lines, the ^{137}Ba magnetization decay is much longer and exhibits pronounced oscillations. Fitting the experimental data to formula (8) provides the oscillation frequency from which we extracted a value of the local magnetic field of $\mu_0 H_{\rm loc} = 7.24$ mT at the ^{137}Ba NQR

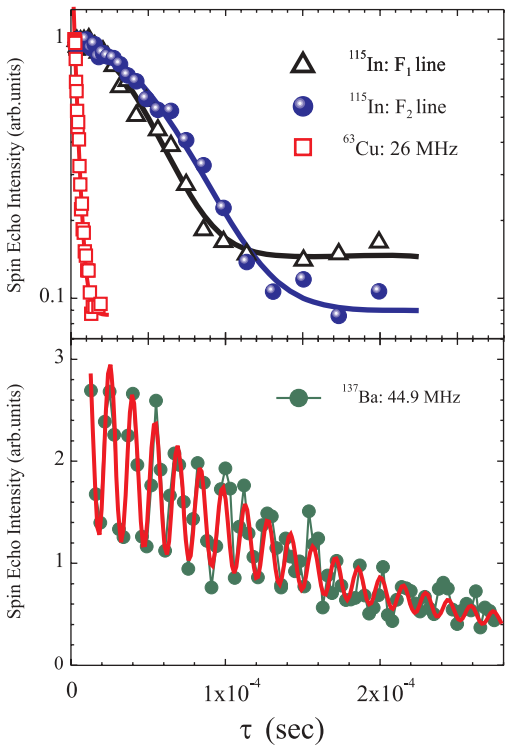

FIG. 10. (Color online) (Top) Spin-echo intensity decay for the NQR lines of ^{115}In: F_1 transition (triangles), F_2 transition (balls), and ^{63}Cu at 26 MHz (squares) in $Ba_3Cu_3In_4O_{12}$ measured at 2.5 K. Solid lines are the best fit to the formula (7) with only the second term for both ^{115}In lines and with only the first term for ^{63}Cu line (see text). (Bottom) Spin-echo intensity decay for the ^{137}Ba NQR line at 44.9 MHz measured at 2.5 K. The solid curve is the best fit to formula (8).

line at 44.9 MHz. This minor local field might be a result of an incomplete cancellation of the supertransferred hyperfine (STHF) and dipolar magnetic field from Cu^I spin at the Ba site. Due to its low value it cannot cause a visible line splitting of the ^{137}Ba NQR spectrum discussed above. A similar situation has been observed in $YBa_2Cu_3O_{6.05}$ (Ref. 8).

It should be mentioned that both supertransferred and dipolar contributions to the magnetic field at the In site induced by spin-polarized Cu^I ions are believed to have opposite signs and might be of the same order of magnitude. Therefore, they can almost cancel each other, resulting in an unobserved presence of minor local magnetic fields in our pure NQR experiments.

5. Zero-field $^{63,65}Cu^I$ NMR

In the frequency range of 50–65 MHz we found a "palisade" of resonance lines (see Fig. 11) which we identified as a zero-field $^{63,65}Cu^I$ NMR spectrum of $Ba_3Cu_3In_4O_{12}$. At first sight its complicated shape points to an existence of several nonequivalent Cu^I positions with varying both EFG and local field values. However, utilizing the simulation program with a direct numerical solution of the spin Hamiltonian for both ^{63}Cu and ^{65}Cu isotopes we succeeded to obtain a reasonable fit to the experimental zero-field spectrum using only two nonequivalent Cu^I positions [Cu^I(a) and Cu^I(b)] resulting in 12 lines (solid lines in Fig. 11). It should be noted that this simulation is a simple "approximation by eye." Since there are too many fitting parameters (see Table II) it is almost impossible to obtain analytically a perfect coincidence with the experimental spectrum. A more careful examination of the experimental spectrum shows that actually we deal with a superposition of NMR spectra for more than two nonequivalent Cu^I positions with close-enough electric and magnetic hyperfine coupling parameters. Interestingly, the existence of mainly two nonequivalent Cu^I sites in the crystal structure of $Ba_3Cu_3In_4O_{12}$ in the magnetically ordered

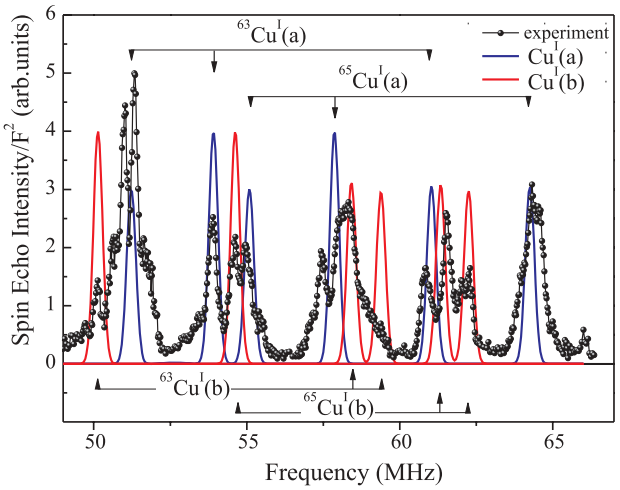

FIG. 11. (Color online) Zero field ^{63,65}Cu NMR of $Ba_3Cu_3In_4O_{12}$ measured at 1.6 K and normalized to the square of frequency. Solid lines represent a theoretical simulation for two nonequivalent Cu^I positions with the parameters given in Table II. The lines corresponding to the central and satellite transitions of ^{63,65}Cu nuclei are shown by long and short arrows, respectively.

TABLE II. Simulation parameters for the Cu^I zero-field spectrum. θ is the angle between the local field direction and the main axis of the EFG (c axis).

Parameter	Cu^I(a)	Cu^I(b)
Local field (T)	4.77	4.82
NQR frequency for ^{63}Cu (MHz)	30.8	23.1
Asymmetry parameter η	0	0.05
Orientation angle θ (deg.)	54	66

state can be easily explained to be a result of (quasi)static nonuniform displacements of Cu^I ions along the cavity in the c direction, which was independently observed by the ^{115}In and, particularly, by the $^{63,65}Cu^{II}$ NQR (see, e.g., Fig. 8). The c-axis displacements of Cu^I ions will vary the EFG at the $^{63,65}Cu^I$ nuclei and the local field, for example, due to a direct variation of the $^{63,65}Cu^I$-Cu^I STHF coupling constants. The crystalline c axis is believed to be a symmetry axis for the electric field on the $^{63,65}Cu^I$ nuclei for any c-axis displacements. Indeed, our fit yields $\eta \approx 0$ for the two nonequivalent positions. Note that the c-axis displacement has most likely a statistical nature since no crystal and/or magnetic superstructure was observed in neutron diffraction experiments in the isostructural compound $Ba_3Cu_3Sc_4O_{12}$ (Ref. 2). In contrast, zero-field NMR is a local probe which is extremely sensitive to slight variations of the local magnetic field and EFG values as well as to their mutual orientation even in the case of statistical displacements.

In any case, we see that the on-site Cu^I direct hyperfine coupling is a main contributor (~50 MHz) to the local field. The on-site Cu direct hyperfine coupling constants at $\mu_{Cu^I} \approx 0.65\mu_B$ (Ref. 2) can be estimated as follows:[10] $A^{\parallel} \approx 140$ MHz, $A^{\perp} \approx 20$ MHz. In other words, the magnetic moments of the Cu^I ions seem to be severely turned away from the c axis in accordance with the fitting data in Table II.

B. Field-sweep NMR

To investigate in detail the ground-state magnetic properties of $Ba_3Cu_3In_4O_{12}$ we performed a series of field-sweep NMR spectrum measurements at 1.6 K at several fixed frequencies in the range of 15–50 MHz. The spacing between pulses was kept fixed at the shortest possible value (28 μs) in order to enable observation of the fast-relaxing ^{63,65}Cu signal (see Sec. III A 4) and to avoid any distortions of the spectra. The typical spectra are presented in Fig. 12 with vertical solid and dashed lines which indicate the position of the Larmor field at a given frequency for ^{115}In and ^{63}Cu nuclei, respectively. Before the field sweeps were recorded the sample was cooled in zero applied magnetic field (ZFC). All spectra consist of two lines: (i) the broad line in the field range of 0–5 T with asymmetric shape ("low-field line") and (ii) the narrow line in the field range 5–7 T ("high-field line").

Let us start our analysis with the low-field line. With increasing frequency in the range of 15–27 MHz the field of maximum intensity of this broad line follows the Larmor field values for both the ^{115}In and the ^{63}Cu nuclei (see Fig. 12, left panel).

This field dependence of the resonance frequency is depicted in Fig. 13 (blue solid triangles and the straight line

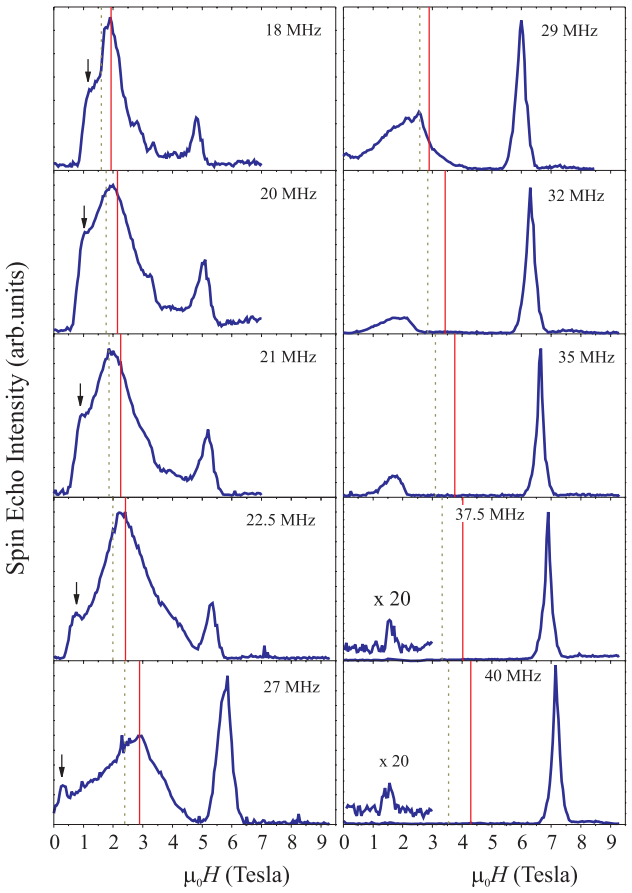

FIG. 12. (Color online) ZFC field-sweep NMR spectra of $Ba_3Cu_3In_4O_{12}$ measured at various fixed frequencies at 1.6 K. Vertical solid and dashed lines indicate the position of the Larmor field at a given frequency for ^{115}In and ^{63}Cu nuclei, respectively. Arrows point to the position of the left shoulder (subline) of the low-field lines (see text).

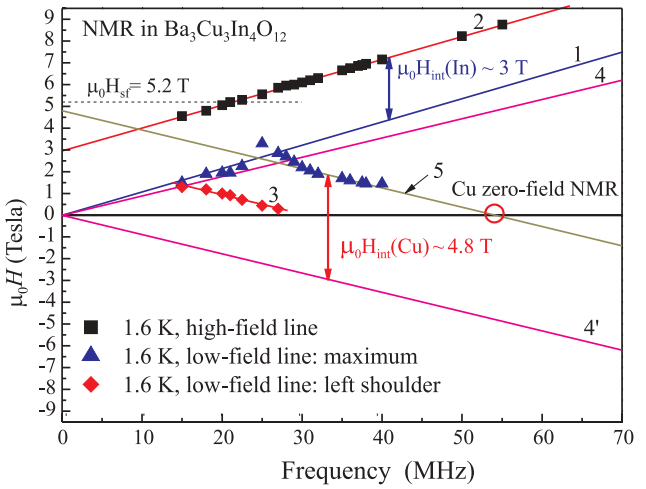

FIG. 13. (Color online) Resonance field vs frequency diagram for $Ba_3Cu_3In_4O_{12}$ extracted from the field-sweep NMR measurements. Symbols are the experimental data. The following straight lines are shown. (1) Larmor line for ^{115}In nuclei: $\mu_0 H_L(^{115}\text{In}) = (1/^{115}\gamma)F_{\text{res}}$, where $(1/^{115}\gamma) = 0.107$; (2) the best linear fit $\mu_0 H_{\text{res}} = k_2 F_{\text{res}} + \mu_0 H_{hf}$ to the experimental data at the maximum of the high-field line, where $k_2 = 0.106(1)$, $\mu_0 H_{hf} = 2.95$ T; (3) the best linear fit $\mu_0 H_{sh} = k_3 F_{\text{res}} + \mu_0 H_0$ to the left shoulder of the low-field line (marked by arrows in Fig. 12), where $k_3 = -0.089(7)$; (4) and (4′) Larmor lines for ^{63}Cu nuclei: $\mu_0 H_L(^{63}Cu) = \pm(1/^{63}\gamma)F_{\text{res}}$, where $1/^{63}\gamma = 0.0887$; (5) the best linear fit $\mu_0 H_{\text{res}} = -(1/^{63}\gamma)F_{\text{res}} + \mu_0 H_0$ to the experimental data at the maximum of the low-field line, where $\mu_0 H_0 = 4.8(4)$ T. The red circle indicates the expected position of the copper zero-field NMR.

No. 1). Since there is not much difference in the gyromagnetic constants for the ^{115}In and ^{63}Cu nuclei (see Table I), the straight lines corresponding to the Larmor condition $\mu_0 H_L(^{115}\text{In}) = (1/^{115}\gamma)F_{\text{res}}$ (line No. 1 in Fig. 13) and $\mu_0 H_L(^{63}\text{Cu}) = (1/^{63}\gamma)F_{\text{res}}$ (line No. 4 in Fig. 13) are close to each other at low frequencies. Indeed, taking into account the uncertainty of the experimental data the exact slope of the experimental data in the frequency range of 15–28 MHz in Fig. 13 cannot easily be determined. This line at frequencies below 27 MHz is composed of ^{115}In and ^{63,65}Cu NMR powder patterns resulting in a very broad intensity distribution. Furthermore, there is a characteristic left shoulder of the low-field line marked by arrows in Fig. 12. It develops into a separate small subline moving linearly towards low fields with increasing frequency. This is shown in Fig. 13 by solid red diamonds and line No. 3, which is the best linear fit $\mu_0 H_{sh} = k_3 F_{\text{res}} + \mu_0 H_0$ to the experimental data, where $|k_3| = 0.089(7)$. This value is almost exactly equal to the reciprocal gyromagnetic constant for ^{63}Cu nuclei: $1/^{63}\gamma = 0.0887$ (Table I). It is worth mentioning that this shoulder completely disappears above 29 MHz and the linear fit (line No. 3) crosses the frequency axis at around 30 MHz, which is close to the value of the $^{63}Cu^{II}$ NQR frequency (see Fig. 8). Thus, we can conclude that the shoulder subline of the low-field line (Fig. 12) is the Zeeman-perturbed Cu NQR from the nonmagnetic Cu^{II} site at low external magnetic fields. In this case the splitting of the NQR transition $\Delta F_{\text{NQR}} = F_{\text{res}} - F_{\text{NQR}}$ is proportional to γH, which is indeed observed in our experiment.

Surprisingly, above 27 MHz the maximum of the low-field line starts to deviate from the Larmor field value rapidly moving in the opposite direction (see Fig. 12, right panel, and Fig. 13). At the same time the intensity of the low-field line decreases drastically. We can assume that the observed behavior originates from the magnetic Cu site in the presence of both an internal field and the external field, which have opposite directions, inducing the resulting Larmor field at the Cu site. The linear fit $\mu_0 H_{\text{res}} = (1/^{63}\gamma)F_{\text{res}} + \mu_0 H_0$ to the experimental data at frequencies 28–40 MHz gives the value of $\mu_0 H_0 = 4.8(4)$ T in perfect agreement with our zero-field Cu^{I} NMR (Fig. 11 and Table II). The extrapolation of this linear fit to higher frequencies crosses the frequency axis at around 54 MHz (see Fig. 13, red circle), which is inside the frequency range of the zero-field Cu^{I} NMR spectrum in $Ba_3Cu_3In_4O_{12}$ (Fig. 11).

Now we have to analyze the high-field line in the observed field-sweep spectra (Fig. 12). The position of the maximum of this line at various fixed frequencies in the range of 15–55 MHz at 1.6 K, 2 K, and 5 K perfectly fits to the linear function $\mu_0 H_{\text{res}} = k_2 F_{\text{res}} + \mu_0 H_{hf}$, where $k_2 = 0.106(2)$, $\mu_0 H_{hf} = 2.95(3)$ T (line No. 2 in Fig. 13). The value of the linear coefficient k_2 is almost exactly equal to the reciprocal gyromagnetic constant for ^{115}In nuclei: $1/^{115}\gamma = 0.107$ (Table I)

so that the line No. 2 is perfectly parallel to the Larmor line for the ^{115}In nuclei (line No. 1 in Fig. 13) in the entire frequency range covered here. It is worth mentioning that at frequencies below 25 MHz the integral intensity of the high-field line is significantly lower than that of the low-field line. However, above 25 MHz when the resonance field of the high-field line exceeds the value of the spin-flip field $\mu_0 H_{sf} = 5.2$ T (Ref. 1), the intensity of the high-field line rapidly increases with frequency accompanied by a dramatic decrease of the low-field line intensity (see Fig. 12, right panel). This remarkable phenomenon enables us to conclude that in the spin-flip phase of $Ba_3Cu_3In_4O_{12}$ all copper spins (Cu^I and Cu^{II}) are aligned along the direction of the external field $H > H_{sf}$, creating a supertransferred hyperfine field at the In nuclei of $\mu_0 H_{hf} = 2.95$ T. Since for all crystallites the directions of the external fields and, hence, all copper spins are the same, the orientation and the value of the hyperfine field at the In site is the same, creating a single-crystal-like effect which results in a relatively narrow high-field line shape in comparison to the low-field one. It is interesting to mention that in the frequency range of 15–25 MHz both low-field and high-field lines coexist, indicating a pronounced coexistence of the mixed-spin phase and the spin-flip phase in $Ba_3Cu_3In_4O_{12}$.

Thus, we see that although the ^{115}In nucleus is hyperfine coupled to three Cu ions which are part of a spin-polarized Cu^I-$2Cu^{II}$ trimer a noticeable local field is induced only at $H \geqslant H_{sf}$. In other words, spin-polarized Cu^I ions produce a negligible contribution to the local field on the ^{115}In nucleus, probably because of an unfavorable ^{115}In-O-Cu^I STHF coupling geometry, and $\mathbf{H}_{hf}(T) \propto \langle \mathbf{S}_2 \rangle$. Hence, the spin-flip field $\mu_0 H_{sf} \approx 5.2$ T in $Ba_3Cu_3In_4O_{12}$ may be related to a singlet-triplet transition in $2Cu^{II}$ dimers, or LS-HS transition in Cu^I-$2Cu^{II}$ trimers in full accordance with predictions of the trimer model.

It is worth noting that, in contrast to the high-field In line which is observed definitely in the spin-flip phase ($\mu_0 H >$ 5.2 T), for the low-field copper line we are in the mixed-spin phase (1.5 T $< \mu_0 H <$ 3 T; see line 5 in Fig. 13), which is in the range of the spin-flop transition for Cu_I spins (Ref. 1). For Cu_I spins in the spin-flop phase their spins are perpendicular to the external field so that the resulting magnetic field on the Cu nuclei is a vector sum of external and the on-site hyperfine fields. Therefore, the contribution to the resulting field from the latter is not constant and depends on the value of the former and the resonance frequency, in general, should not be proportional to γ. However, for the small range of the fields around maximum line intensity we can assume that the hyperfine on-site contribution is constant, resulting in the linear dependence (line 5 in Fig. 13). However, due to the reason mentioned above, this linear approximation to the experimental points is not as perfect as the line 2, providing only a rough estimate for the frequency range of the zero-field NMR Cu_I signal to search for.

Finally, we investigated the evolution of the high-field line with temperature at a fixed frequency of 35.0 MHz. The results are presented in Fig. 14. Surprisingly, the high-field line does not disappear at the Néel temperature $T_N = 12.7$ K but exists, albeit with decreasing intensity, far above T_N. Because of a poor signal-to-noise ratio it was not possible to observe this line above 20 K. The difference of the field at maximum intensity

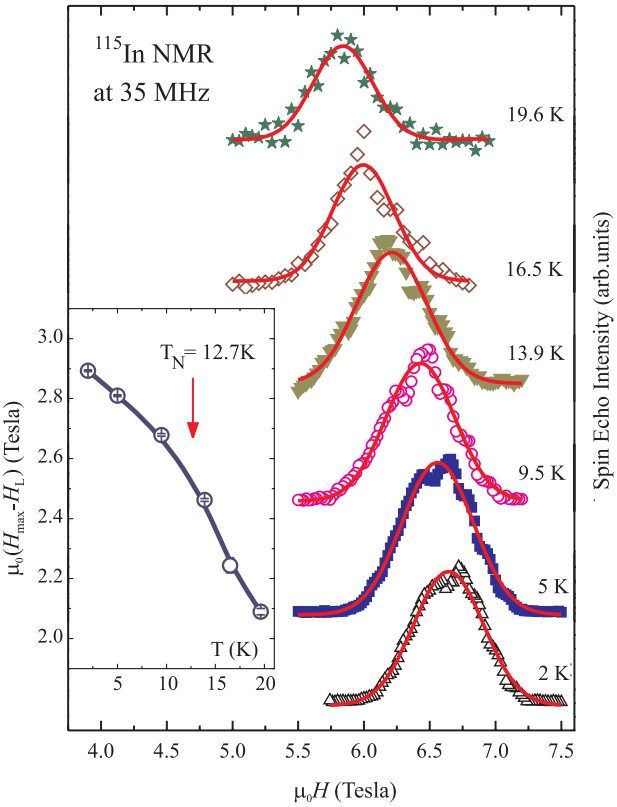

FIG. 14. (Color online) Temperature evolution of the ^{115}In high-field line in $Ba_3Cu_3In_4O_{12}$ measured at 35 MHz. The position of the Larmor field $\mu_0 H_L(35\ \text{MHz}) = 3.75$ T coincides with the position of the ordinate axis. (Inset) Temperature dependence of the maximum of the ^{115}In high-field line. The red arrow indicates the position of the Néel temperature in $Ba_3Cu_3In_4O_{12}$.

$\mu_0 H_{max}$ and the Larmor field of the ^{115}In nuclei at 35.0 MHz ($\mu_0 H_L = 3.75$ T) decreases gradually in the temperature range of 2–20 K (see inset in Fig. 14) but still exceeds the value of 2 T at 19.6 K. This result demonstrates that a significant hyperfine magnetic field at the In site remains at $T > T_N$, indicating that short-range magnetic order is existing well above T_N in $Ba_3Cu_3In_4O_{12}$. This is in agreement with the observation in Ref. 1 that only 15.4% of the magnetic entropy $\Delta S_{mag} =$ 17.29 J/mol K are released at T_N. The existence of a magnetic contribution to the heat capacity at temperatures much higher than T_N was found in $Ba_3Cu_3Sc_4O_{12}$ as well.[2]

It should be mentioned that if one takes the value of the quadrupole frequency of ^{115}In from our NQR data as 8.71 MHz (Fig. 5) then the quadrupole satellite structure (at least of the first order) should be observed in the ^{115}In field spectra. However, we do not see it in the high-field line (Fig. 12). Also, in the papers of Koteswararao *et al.* and Gippius *et al.*[2] the authors did not observe any pronounced quadrupole features in the ^{45}Sc NMR spectra in the Sc-based isostructural compound at relatively high fields of 6–7 T. Koteswararao *et al.*[2] argued that there are two types of In sites: One is in nondistorted octahedra with almost zero quadrupole constant, and the second is in slightly distorted octahedra with $\nu_Q \sim 400$ kHz. From this point of view we can state that our In-based compound also consists of two types of InO_6

octahedra, one with almost perfect octahedral symmetry and another with distortions. Thus, we can conclude that our ^{115}In NQR spectra originate from the latter while the high-field ^{115}In NMR line comes from the former. Due to the relatively high quadrupole constant in the distorted InO_6 octahedra ($\nu_Q = 8.71$ MHz) the NMR line from these In sites is very broad and the quadrupole structure is almost invisible in the field-sweep spectra. Indeed, we can observe only a very weak broad signal to the right of the main high-field In line in the right panel in Fig. 12.

IV. SUMMARY AND CONCLUSIONS

We propose the paper chains in $Ba_3Cu_3In_4O_{12}$ or $Ba_3Cu_3Sc_4O_{12}$ to be a chain system of Cu^I-$2Cu^{II}$ trimers. Theoretical estimates of different exchange integrals[2] point to a LS $S = 1/2$ ground state of the trimer which implies a nonmagnetic spin-singlet $2Cu^{II}$-dimer state. Close to this ground state one finds a low-lying HS $S = 3/2$ state in the energy spectrum. The model immediately explains low-temperature Schottky-type anomalies and other peculiarities of the specific heat in both paper-chain compounds. The LS-HS quasidegeneracy as a result of an antiferroferromagnetic $J_{22}^{\perp}$-J_{12} competition explains the very low magnitude of the magnetic field $\mu_0 H_S$ necessary to saturate the magnetization, 5 T in $Ba_3Cu_3In_4O_{12}$ and 8 T in $Ba_3Cu_3Sc_4O_{12}$, respectively.[1,2,4] Furthermore, it predicts several spin-flop- and spin-flip-like transitions which are indeed clearly seen at several critical fields $H < H_S$ for $T < T_N$.

Our main experimental results are related to extensive nuclear resonance NQR-NMR measurements for the copper, indium, and barium nuclei in $Ba_3Cu_3In_4O_{12}$, which provide strong support for the model of Cu^I-$2Cu^{II}$ trimers.

Two different types of ^{63,65}Cu nuclear resonance spectra were observed in the magnetically ordered state in $Ba_3Cu_3In_4O_{12}$ at zero external magnetic fields: (i) a pure NQR spectrum in the frequency range of 24–30 MHz and (ii) a zero-field NMR spectrum in the frequency range of 50–65 MHz. This result unambiguously indicates that one of the two types of copper ions in $Ba_3Cu_3In_4O_{12}$ is in a nonmagnetic spin state below T_N.

We interpret the two different types of ^{63,65}Cu nuclear resonance spectra to be the NQR spectrum of Cu^{II} ions which are part of a nonmagnetic spin-singlet $2Cu^{II}$ dimer and the zero-field NMR spectrum of spin-polarized Cu^I ions, respectively. Actually this is a direct experimental verification of the Cu^I-$2Cu^{II}$-trimer model.

The formation of the spin singlets on Cu^{II} ions makes it possible to exclude magnetic frustration in paper-chain systems. Magnetic frustration effects were already discarded by the authors of Ref. 1 within their model of an orthogonal spin ordering. However, it is impossible to reconcile our observation of a pure Cu NQR with the latter model of orthogonal spin ordering. It is worth noting that the observation of a pure Cu^{2+} NQR spectrum is a rare case among the antiferromagnetic cuprates. Indeed, the values of local magnetic fields at magnetic Cu sites typically observed in antiferromagnetic cuprates below T_N are in the range of several Teslas, that is 7.9 T in $La_2CuO_{4-\delta}$ (Ref. 13), 12.16 T in CuO (Ref. 14), and 7.67 T in $YBa_2Cu_3O_6$ (Ref. 15). These strong internal magnetic fields existing at the Cu^{2+} sites lead to the formation of zero-field NMR spectra prohibiting the observation of a pure Cu NQR spectrum in the magnetically ordered state.

The zero-field $^{63,65}Cu^I$ NMR spectrum proves the occurrence of at least two nonequivalent Cu^I sites in the crystal structure of $Ba_3Cu_3In_4O_{12}$ in the magnetically ordered state which can be easily explained to be a result of (quasi)static nonuniform displacements of the Cu^I ions across the cavity along the c direction due to a peculiar local magnetostriction effect, which was independently observed by ^{115}In and $^{63,65}Cu^{II}$ NQR.

No magnetic splittings of the ^{115}In, ^{137}Ba, and $^{63,65}Cu^{II}$ NQR lines were observed. Therefore, we are able to estimate the upper bound of supertransferred and dipole fields induced by spin-polarized Cu^I ions at the probing nuclei to be of the order of 0.01 T. Our spin-spin relaxation measurements provide an additional independent evidence for negligible values of the local magnetic field at the Cu^{II} and In sites in $Ba_3Cu_3In_4O_{12}$. Only in the case of the Ba site we identified a minor local field of 7.24 mT.

In the spin-flip phase of $Ba_3Cu_3In_4O_{12}$ ($H > H_{sf}$ with $\mu_0 H_{sf} = 5.2$ T) the high-field ^{115}In NMR spectra were observed. This enables us to determine the hyperfine magnetic field ($\mu_0 H_{sf} \approx 3$ T) at the In site in the spin-flip phase induced by spin-polarized Cu ions. It is worth noting some similarity between our ^{115}In NMR data and that of ^{45}Sc NMR in $Ba_3Cu_3Sc_4O_{12}$[2] although the ^{45}Sc NMR spectra in $Ba_3Cu_3Sc_4O_{12}$ were measured mostly below or at the border of the spin-flip transition at $\mu_0 H_{sf} \approx 7$ T. Our observation of the high-field ^{115}In NMR spectra above T_N indicates that a specific short-range magnetic order exists well above T_N in $Ba_3Cu_3In_4O_{12}$, in full accordance with the predictions of the trimer model.

In conclusion, our microscopic model of Cu trimers together with our extensive NQR and NMR measurements provides a comprehensive understanding of the magnetic and electronic properties of the paper-chain compound $Ba_3Cu_3In_4O_{12}$.

ACKNOWLEDGMENTS

This work was partially supported by the RFBR Grants No. 10-02-00021, No. 10-02-96032, No. 11-02-92707-IND, and No. 12-02-01039. N.B., W.K., and A.G. acknowledge the support of the DFG via TRR 80 (Augsburg-Munich).

[1] O. S. Volkova, I. S. Maslova, R. Klingeler, M. Abdel-Hafiez, Y. C. Arango, A. U. B. Wolter, V. Kataev, B. Büchner, and A. N. Vasiliev, Phys. Rev. B **85**, 104420 (2012).

[2] B. Koteswararao, A. V. Mahajan, F. Bert, P. Mendels, J. Chakraborty, V. Singh, I. Dasgupta, S. Rayaprol, V. Siruguri, A. Hoser, and S. D. Kaushik,

J. Phys.: Condens. Matter **24**, 236001 (2012); A. A. Gippius, V. P. Denisov, V. V. Moshchalkov, Yu. M. Petrusevich, O. P. Revokatov, E. V. Antipov, A. L. Kharlanov, L. M. Kovba, and L. N. Lykova, Sov. Phys. JETP **68**, 1229 (1989).

[3]D. H. Gregory, P. R. Mawdsley, S. J. Barker, W. Daniell, and D. P. Weston, J. Mater. Chem. **11**, 806 (2001).

[4]S. E. Dutton, M. Kumar, Z. G. Soos, C. L. Broholm, and R. J. Cava, J. Phys.: Condens. Matter **24**, 166001 (2012).

[5]A. A. Gippius, E. N. Morozova, A. S. Moskvin, A. V. Zalessky, A. A. Bush, M. Baenitz, H. Rosner, and S.-L. Drechsler, Phys. Rev. B **70**, 020406(R) (2004); A. A. Gippius, A. S. Moskvin, and S.-L. Drechsler, *ibid*. **77**, 180403 (2008); N. Büttgen, H.-A. Krug von Nidda, L. E. Svistov, L. A. Prozorova, A. Prokofiev, and W. Assmus, *ibid*. **76**, 014440 (2007); N. Büttgen, W. Kraetschmer, L. E. Svistov, L. A. Prozorova, and A. Prokofiev, *ibid*. **81**, 052403 (2010).

[6]L. E. Aleandri and H. G von Schnering, J. Less-Common Met. **156**, 181 (1989).

[7]A. L. Kharlanov, N. R. Khasanova, M. V. Paramonova, E. V. Antipov, L. N. Lykova, and L. M. Kovba, Zh. Neorg. Khim. **35**, 3067 (1990) [in Russian].

[8]A. Lombardi, M. Mali, J. Roos, and D. Brinkmann, Phys. Rev. B **53**, 14268 (1996).

[9]R. L. Martin, Phys. Rev. Lett. **75**, 744 (1995).

[10]S. Renold, S. Pliberšek, E. P. Stoll, T. A. Claxton, and P. F. Meier, Eur. Phys. J. B **23**, 3 (2001).

[11]M. Bloom and R. E. Norberg, Phys. Rev. **93**, 638 (1954).

[12]E. L. Hahn and B. Herzog, Phys. Rev. **93**, 639 (1954).

[13]K. Ueda, T. Sugata, Y. Kohori, T. Kohara, Y. Oda, M. Yamada, S. Kashiwai, and M. Motoyama, Solid State Commun. **73**, 49 (1990).

[14]T. Tsuda, T. Shimizu, H. Yasuoka, K. Kishio, and K. Kitazawa, J. Phys. Soc. Jpn. **57**, 2908 (1988).

[15]H. Yasuoka, T. Shimizu, T. Imai, S. Sasaki, Y. Ueda, and K. Kosuge, Hyperfine Interact. **49**, 167 (1989).